

# End-binding protein 1 controls signal propagation from the T cell receptor

Noa B Martín-Cófreces<sup>1,2</sup>,  
Francesc Baixauli<sup>1,2</sup>, María J López<sup>1,2</sup>,  
Diana Gil<sup>3</sup>, Alicia Monjas<sup>4</sup>,  
Balbino Alarcón<sup>4</sup> and  
Francisco Sánchez-Madrid<sup>1,2,\*</sup>

<sup>1</sup>Servicio de Inmunología, Hospital Universitario de la Princesa, Universidad Autónoma de Madrid, Instituto Investigación Sanitaria Princesa (IIS-IP), Madrid, Spain, <sup>2</sup>Departamento de Biología Vasculare e Inflamación, Centro Nacional de Investigaciones Cardiovasculares (CNIC), Madrid, Spain, <sup>3</sup>Department of Immunology, College of Medicine, Mayo Clinic, Rochester, MN, USA and <sup>4</sup>Centro de Biología Molecular Severo Ochoa (CBMSO), Consejo Superior de Investigaciones Científicas-Universidad Autónoma de Madrid, Madrid, Spain

**The role of microtubules (MTs) in the control and dynamics of the immune synapse (IS) remains unresolved. Here, we show that T cell activation requires the growth of MTs mediated by the plus-end specific protein end-binding 1 (EB1). A direct interaction of the T cell receptor (TCR) complex with EB1 provides the molecular basis for EB1 activity promoting TCR encounter with signalling vesicles at the IS. EB1 knockdown alters TCR dynamics at the IS and prevents propagation of the TCR activation signal to LAT, thus inhibiting activation of PLC $\gamma$ 1 and its localization to the IS. These results identify a role for EB1 interaction with the TCR in controlling TCR sorting and its connection with the LAT/PLC $\gamma$ 1 signalosome.**

*The EMBO Journal* (2012) 31, 4140–4152. doi:10.1038/emboj.2012.242; Published online 24 August 2012

**Subject Categories:** signal transduction; immunology

**Keywords:** cell signalling; cytoskeleton; microtubule dynamics; T cell activation; vesicular trafficking

## Introduction

The T cell receptor (TCR) complex is exposed on the surface of T cells, and is formed by heterodimers of ligand-binding subunits, either TCR- $\alpha$  and TCR- $\beta$  (in  $\alpha\beta$  T cells) or TCR- $\gamma$  and TCR- $\delta$  (in  $\gamma\delta$  T cells), which associate with the signal-transducing subunits CD3 $\gamma$ , - $\delta$ , - $\epsilon$  and - $\zeta$  (van der Merwe and Dushek, 2011). The cytoplasmic tails of CD3 $\gamma$ , - $\delta$  and - $\epsilon$  contain a single copy of a motif called ITAM (immune-receptor tyrosine-based activation motif), whereas CD3 $\zeta$  contains three ITAMs. ITAMs are phosphorylated upon TCR stimulation by kinases of the src family. Phosphorylated ITAMs are docking sites for SH2-domain containing proteins (Schamel *et al*, 2006). ITAM

\*Corresponding author. Laboratorio de Comunicación Intercelular, Servicio de Inmunología, Instituto de Investigación Sanitaria Princesa, Planta 1, Hospital de La Princesa, Diego de León 62, Madrid 28006, Spain. Tel.: +34 915202307; Fax: +34 915202374; E-mail: fsanchez.hlpr@salud.madrid.org

Received: 22 March 2012; accepted: 25 July 2012; published online: 24 August 2012

phosphorylation is necessary for the polarization of the centrosome to the immune synapse (IS; Lowin-Kropf *et al*, 1998), which is therefore dependent on Lck and Fyn tyrosine kinase activity (Lowin-Kropf *et al*, 1998; Martín-Cofreces *et al*, 2006; Etienne-Manneville, 2010). Centrosome movement is dependent on the dynein/dynactin motor, which allows sustained TCR activation (Martín-Cofreces *et al*, 2008) and polarized secretion (Huse *et al*, 2008). The movement of the centrosome carries cytoplasmic organelles, including the Golgi, multivesicular bodies and the mitochondria network, towards the IS (Calabia-Linares *et al*, 2011), contributing to TCR signalling and IS formation (Baixauli *et al*, 2011).

The specific function of microtubules (MTs) in T cell activation is poorly understood. MTs are large polymers of  $\alpha/\beta$ -tubulin dimers that control intracellular organelle distribution and trafficking (Etienne-Manneville, 2010). MTs show intrinsic polarity, with minus-ends that can anchor to the centrosome to avoid rapid de-polymerization (Li and Gundersen, 2008). MT plus-ends show dynamic instability, being able to switch between growing and shrinkage phases. End-binding proteins (EBs) are highly conserved and ubiquitous plus-end tracking proteins (+TIP) (Tirnauer and Bierer, 2000). The three EBs (EB1, 2 and 3) are small dimeric proteins that contain an N-terminal calponin homology (CH) domain, which is able to bind to MTs. These proteins possess, at their C-terminus, a flexible acidic tail that contains the sequence EEY/F, required for self-inhibition and binding to various partners, that can control MT growth (Akhmanova and Steinmetz, 2008; Manna *et al*, 2008).

In this study, EB1 was found to bind to the CD3 ITAMs. Knockdown of EB1 in T cells prevents TCR clustering at the IS and the correct phosphorylation of LAT and PLC $\gamma$ 1. We found that EB1 regulates vesicular trafficking at the IS and therefore the connection between the TCR and downstream signalling molecules, such as LAT/PLC $\gamma$ 1. These results suggest that TCR-EB1 interaction may play a dual role at the IS, controlling both TCR sorting and its encounter with the LAT/PLC $\gamma$ 1 signalosome.

## Results

### **EB1 directly interacts with the CD3 ITAMs through its four-helix bundle**

To identify new interacting partners of the TCR complex, we used a yeast two-hybrid SOS-recruitment system to screen for CD3 $\epsilon$  cytoplasmic tail-binding proteins. EB1 was identified in this screening (Supplementary Table S1). The isolated cDNA encodes the C-terminal third of EB1 (82 amino acids). To confirm EB1-CD3 $\epsilon$  interaction, we performed pull-down assays with GST-EB1 fusion protein in COS cells transfected with different CD3 subunits. CD3 $\epsilon$  and CD3 $\zeta$  were recovered but not CD3 $\gamma$  or CD3 $\delta$  (Figure 1A). GST-EB1 also co-precipitated a purified cytoplasmic fragment of CD3 $\zeta$  (Supplementary Figure S1A), thus suggesting that EB1 interaction with CD3 subunits is direct.

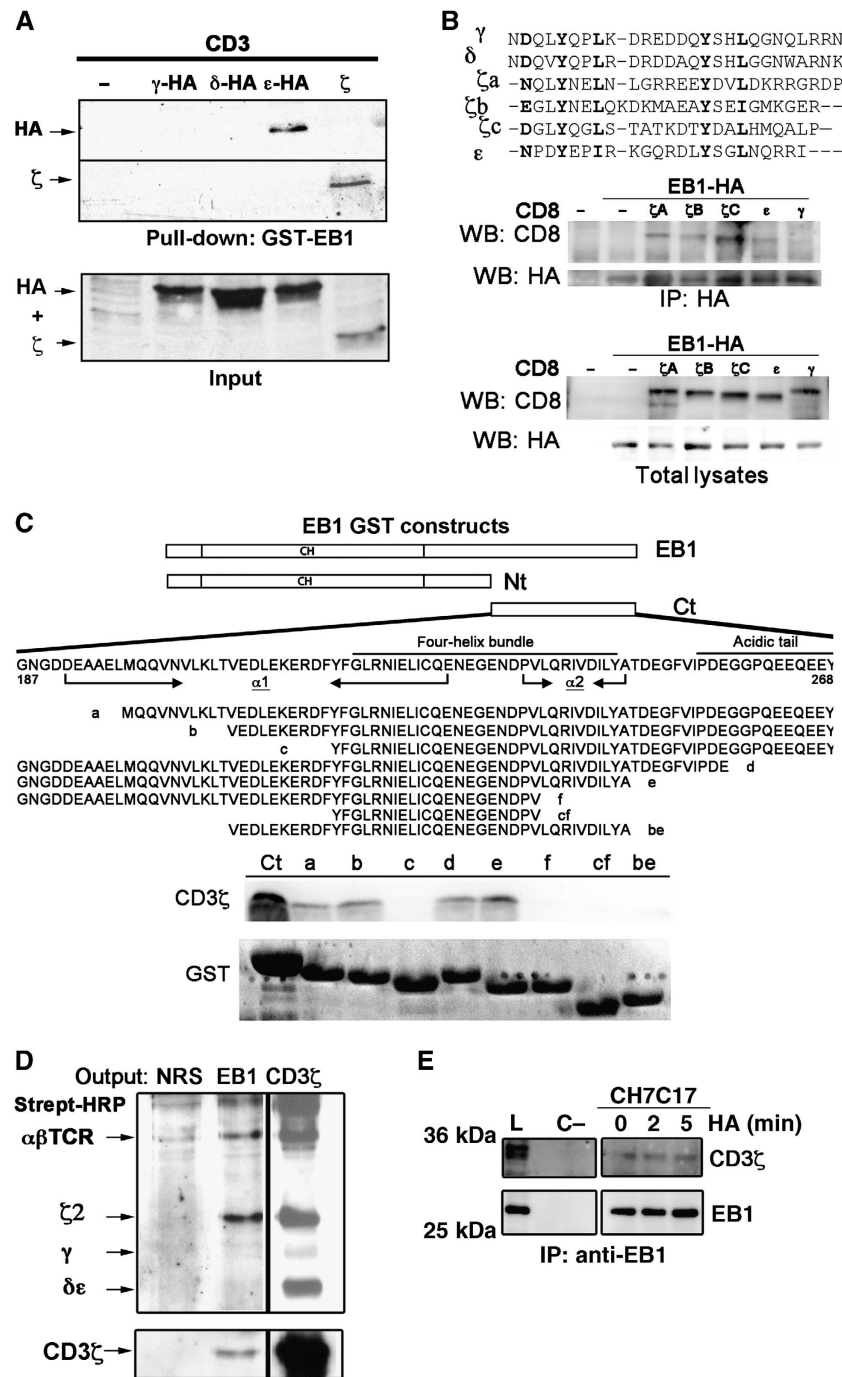


**Figure 1** ITAM-dependent interaction of CD3 with EB1. (A) Pull-down of HA-tagged CD3 subunits with full-length GST-EB1 in co-transfected COS cells. A representative experiment out of three independent experiments is shown. (B) Co-immunoprecipitation of HA-tagged, full-length EB1 with chimeras of the CD8 $\alpha$  extracellular region and the depicted CD3 ITAM sequences. A representative experiment out of three independent experiments is shown. (C) Pull down with the depicted GST-EB1 C-terminal regions of CD3 $\zeta$  from the 2B4 mouse T cell hybridoma and human Jurkat T cell lines. A representative experiment out of five independent experiments is shown. (D) Co-immunoprecipitation of EB1 and surface TcR/CD3 in Jurkat T cells. Biotinylated cells were lysed and subjected to immunoprecipitation with anti-EB1 or CD3 $\zeta$  antibodies. Samples were analysed in the same gel. The image shown in the figure is a composition from two autoradiographs of different time exposure. (E) Co-immunoprecipitation of EB1 with anti-CD3 $\zeta$  in the human CH7C17 T cell line stimulated as indicated with HA-pulsed Hom2 cells (ratio 10:1) in non-reducing conditions; C-, immunoprecipitation with control antibody. A representative experiment out of four independent experiments is shown. Figure source data can be found with the Supplementary data.

ITAMs are the shared regions in the cytoplasmic tails of CD3 $\epsilon$  and CD3 $\zeta$ . Therefore, we assessed whether EB1 interacts with CD3 $\epsilon$  and CD3 $\zeta$  ITAMs using chimeric fusion proteins of CD8 $\alpha$  with each of the three CD3 $\zeta$  ITAMs

( $\zeta$ A,  $\zeta$ B and  $\zeta$ C), or the cytoplasmic tail of CD3 $\epsilon$ . EB1 strongly co-precipitated with each of the three ITAMs from CD3 $\zeta$  (CD8- $\zeta$ C, CD8- $\zeta$ A and CD8- $\zeta$ B) as well as with CD8- $\epsilon$ , but not with CD8 $\gamma$  (Figure 1B). Therefore, the specificity for the

ITAMS of CD3 $\zeta$  and  $\epsilon$  can be explained by the sequence of these ITAMs, which are less acidic than the ITAMs of CD3 $\gamma$  and  $\delta$  (Figure 1B).

To characterize the CD3-binding site in EB1, we generated a panel of GST fusion proteins (Figure 1C). As predicted from the two-hybrid screen, CD3 bound to a construct, GST-Ct, which contained the C-terminal 82 amino acids of EB1. The first half of the  $\alpha 1$  helix is not required for CD3 binding, since deletion of the first 10 or 20 amino acids (*a* and *b* constructs) did not prevent the EB1–CD3 interaction. Likewise, the acidic tail seems to be unnecessary since deletions *d* and *e* did not affect the interaction. However, CD3–EB1 interaction was abrogated by simultaneous elimination of the acidic tail and half of the  $\alpha 1$  helix (deletion *be*) or by either complete deletion of helix  $\alpha 2$  or most of helix  $\alpha 1$  (deletions *f* and *c*). These findings indicate that CD3 binds to the four-helix bundle of EB1.

To analyse whether the CD3–EB1 interaction takes place in T cells, EB1 was immunoprecipitated from murine thymocytes and spleen T cell lysates. EB1 was found associated with CD3 $\zeta$  in cells from both organs (Supplementary Figure S1B). To study whether TCR stimulation affects CD3 $\zeta$  interaction with EB1, anti-CD3-stimulated thymocytes and spleen T cells were immunoprecipitated with anti-CD3 $\zeta$ . EB1 co-immunoprecipitated with the TCR in both cell lysates, independently of CD3 stimulation (Figure S1C). When EB1 immunoprecipitations were carried out with surface-biotinylated Jurkat T cells, two major biotinylated bands were detected, corresponding to the CD3 $\zeta$  homodimer and the TCR $\alpha/\beta$  heterodimer, together with weak signals for CD3 $\gamma$ , CD3 $\delta$  and CD3 $\epsilon$  (Figure 1D). This result points to an EB1 association to a partial TCR complex that contains TCR $\alpha\beta$  and CD3 $\zeta$ . The effect may be due to a multichain immune receptor oligo-oligomerization, where the TCR and CD3 subunits dissociate upon stimulation (Sigalov, 2006). Alternatively, it could be due to a different rate of degradation for the TCR expressed on the surface, as TCR $\alpha\beta$  degrades faster than CD3 chains in non-stimulated cells (San Jose and Alarcon, 1999). Since the association of EB1 with TCR $\alpha\beta$  and CD3 $\zeta$  is detected in non-stimulated T cells (Figure 1D), this interaction may be involved in the trafficking of the most rapidly degraded TCR subunits from the plasma membrane.

To further analyse whether EB1 binding to CD3 $\zeta$  was altered by stimulation, CD3 $\zeta$  was immunoprecipitated from primary CD8+ OT-I transgenic T cells stimulated by OVA antigen-loaded T2kb cells. The recovery of EB1 was similar with or without stimulation (Figure S1D). Moreover, in the mouse T cell hybridoma 2B4, stimulation with anti-CD3 $\epsilon$ +CD28 antibodies did not increase the association of EB1 with the TCR. Effective stimulation in these assays was confirmed by reprobating the membrane with a phosphospecific antibody, revealing that TCR triggering induced a clear increase in the tyrosine phosphorylation of CD3 $\zeta$  (Figure S1E). Finally, CD3 $\zeta$  homodimer was co-precipitated by EB1 immunoprecipitation in CH7C17 T cells activated or not with HA antigen (Figure 1E). These results indicate that EB1 interacts constitutively with the TCR in T cells, independently of their phosphorylation state.

#### **EB1 localizes at the plus-ends of MTs in the IS**

The localization of EB1 during IS formation in activated T cells was assessed in a model of antigen-specific presentation.

Primary CD4+ T cells from OT-II transgenic mice were isolated and conjugated with TNF- $\alpha$ -activated, bone marrow-derived dendritic cells (DCs). In these conjugates, T cells are observed as small, round cells. Cell morphology and IS formation were monitored by F-actin staining. EB1 was detected at the tips of MTs in both the T cell and the DC. In the OVA-stimulated T cells, EB1 strongly decorated the ends of MT emerging from the polarized MT-organizing centre (MTOC) (yellow arrow, Figure 2A and Supplementary Figure S2A), being closely apposed to the cortical F-actin at the IS. This localization suggests a possible role of highly EB1-enriched MT plus-ends as docking structures for maintaining the MTOC at the IS. To further assess EB1 localization during IS formation, we conjugated human polyclonal, primary T lymphoblasts with either control or SEE-pulsed Raji B cells (antigen-presenting cell, APC; Figure 2B). In the absence of SEE, T lymphoblasts localize their MTOC at the uropod (U). In this condition, endogenous EB1 was clearly observed both at the MTOC (yellow arrow) and at points that correspond to the ends of MTs (white arrowheads). The confocal plane shown for SEE-stimulated conjugates reveals the polarized MTOC localized at the IS. The points of EB1 staining can be observed near the CD3 $\zeta$  cluster. The 3D reconstructions of the boxed areas in merged images allow observation of different planes, from the internal MTOC area to the zone just beneath the plasma membrane, marked by CD3 $\zeta$ . Points of EB1 staining are observed in all planes, co-localizing with CD3 $\zeta$ -enriched intracellular clusters and partially co-localizing with CD3 $\zeta$  in the more external planes of the 3D reconstruction (white arrows, right panels in Figure 2B).

We further analysed EB1 localization during IS formation in centrosomes isolated by fractionation through sucrose gradients. GCP3 protein was used as a specific marker of centrosomal fractions (Bettencourt-Dias and Glover, 2007). Equivalent volumes of specific fractions were loaded on the gel, revealing an increased content of EB1 protein in the centrosomal fractions of activated T lymphocytes (Figure 2C). EB1 at the centrosome is essential to configure a radial array of MTs (Askham *et al*, 2002). Indeed, the increase of EB1 in the centrosomal fractions points to an increase in the polymerization of MTs from the centrosome. Therefore, EB1 localization in the plus-ends of MTs and in the centrosome upon T cell activation suggests a role for EB1 in the regulation of MT dynamics at the IS.

#### **EB1 guides MT dynamics at the IS**

To explore the role of EB1 as a plus-end tracking protein at the IS, we analysed whether MTs are actively polymerized at the IS. Growth of MTs from the polarized MTOC was detected in antigen-specific cell conjugates of CH7C17 Jurkat cells and HA-pulsed APCs using EB1-GFP, imaging the confocal plane where the MTOC localized at the interface with the APC (Figure 3A; Supplementary Movie S1). EB1-GFP has been previously used to enable tracking of MT growth by TIRF microscopy (Grigoriev and Akhmanova, 2010) during T cell spreading over an activating anti-CD3+anti-CD28 surface (Bunnell *et al*, 2001). In this system, the EB1-GFP-labelled MT plus tips appear very soon after cells make contact with the surface, and MTOC polarization (white arrow in Figure 3B; Supplementary Movie S2) is visualized within minutes. EB1-GFP is observed at the MTOC co-localizing with tubulin-Cherry rapidly upon T cell spreading



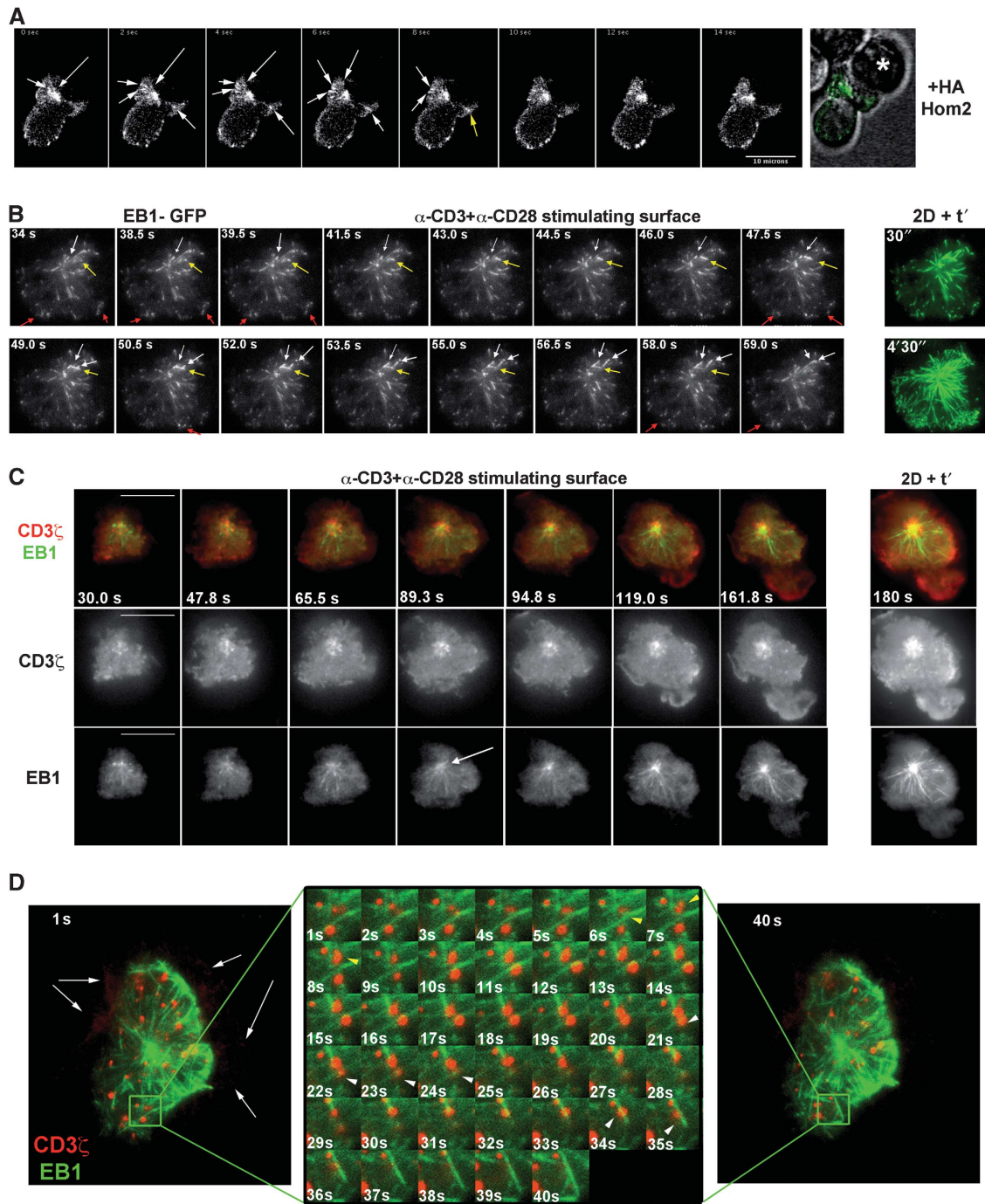


**Figure 3** Microtubule dynamics are driven by EB1 at the IS. (A) EB1-GFP-expressing CH7C17 T cells were conjugated with HA-pulsed APCs and tracked by confocal fluorescence microscopy. A single confocal plane is shown. Images were taken every 2 s. The merged image at the right shows DIC and GFP fluorescence (green). \*, HA-loaded Hom2 B cell. A representative cell conjugate from out of at least three independent experiments is shown. (B) EB1-GFP-expressing CH7C17 cells were allowed to settle on anti-CD3 plus anti-CD28 coated glass-bottomed chambers and images were taken every 500 ms by TIRF microscopy at a penetrance of 150 nm. A representative cell from out of three independent experiments is shown. (C) Jurkat T cells expressing EB1-mGFP (green) and CD3 $\zeta$ -mCherry (red) were treated as in (B) and analysed by TIRFM. Images were taken every 99 ms at a penetrance of 90 nm. White arrow, centrosome. Bar, 5  $\mu$ m. A representative cell from out of at least three independent experiments is shown. (D) Jurkat T cells co-expressing EB1-GFP (green) and CD3 $\zeta$ -Cherry (red) were plated on anti-CD3 plus anti-CD28 coated glass-bottomed chambers and analysed by TIRFM. Images were taken every 1 s at a penetrance of 150 nm. The central panel shows magnified views of a time-lapse sequence of the boxed region between 1 s (left) and 40 s (right). Yellow arrowheads: vesicles appearing at the TIRF plane. White arrowheads: vesicles disappearing from the TIRF plane. White arrows: CD3 $\zeta$  microclusters.

area (red arrows in Figure 3B; Supplementary Movie S2) and even crossing over the central area (yellow arrow in Figure 3B; Supplementary Movie S2). These results point to MTOC polarization as a mechanism for facilitating EB1-

driven polymerization of MTs at the IS, providing a dynamic meshwork for intracellular transport.

To analyse the relationship between MT dynamics and intracellular transport, CD3 $\zeta$  dynamics was tracked with

CD3 $\zeta$ -Cherry, which was found both in microclusters attached to the activating surface and in vesicles (Supplementary Figure S3; Supplementary Movie S3). EB1-GFP and CD3 $\zeta$ -Cherry are observed at the cell surface during spreading and CD3 $\zeta$ -Cherry signal increases at a central cluster corresponding to the later localization of the polarized MTOC (Figure 3C; Supplementary Movie S4). When using a penetrance depth of 90 nm in total internal reflection fluorescence microscopy (TIRFM), microclusters are mainly observed, whereas at 110 nm vesicles are also imaged (Figure 3C; Supplementary Figure S3; Supplementary Movies S3 and S4) and for a penetrance depth of 150 nm, vesicles were mainly on the focus plane (Figure 3D; Supplementary Movie S5). CD3 $\zeta$ + vesicles co-localized with the EB1-marked MT tips during T cell spreading over the activating surface (Figure 3D). These vesicles entered and exited the TIRF focal plane at sites of active MT growth (yellow and white arrowheads, respectively). These results indicate that CD3+ vesicles preferentially use the observed areas of high MT dynamics to move and accumulate.

### **EB1 controls the movement of CD3 $\zeta$ -Cherry-containing vesicles at the IS**

To assess the function of EB1 in the movement of the CD3 $\zeta$ -Cherry-enriched vesicles, EB1 was specifically knocked down in CH7C17 T cells (Supplementary Figure S4). Tracking of vesicle movement by TIRFM in cells plated on stimulating surfaces revealed that movement of CD3 $\zeta$ -Cherry vesicles at the central area of the T cell was impaired in EB1-depleted cells and that these vesicles were mostly displaced to the periphery (Figure 4A; Supplementary Movie S6). This is illustrated by projecting the time lapse on the XY plane ( $2D + t'$ ), which details the areas where the CD3 $\zeta$ + vesicles have been moving (Figure 4B). The time projection on Figure 4C shows that the trajectories of the vesicles in EB1-silenced cells were irregular, in contrast with control cells. Therefore, these data indicate an EB1-dependent, specific control of CD3 $\zeta$  vesicle movement at the IS. To further analyse the role of EB1 in CD3 $\zeta$  positioning at the IS, EB1 expression was silenced in SEE-specific human T lymphoblasts and J77 Jurkat cells (Supplementary Figure S4B and C). Cell conjugates were formed with SEE-pulsed APCs, and analysed for CD3 $\zeta$  accumulation at the IS. Although in EB1-depleted cells CD3 $\zeta$  can be found at the contact area with the APC (Supplementary Figure S5), its clustering at the central area of the IS is impaired (Figure 4D; Supplementary Figure S5). Hence, CD3 $\zeta$  was found at the periphery of the contact area, correlating with the observed trajectories of the vesicles in EB1-silenced cells. Indeed, the mean fluorescence intensity per area at the IS was decreased in EB1-silenced cells (Figure 4D).

### **EB1 regulates the interaction of the TCR and LAT/PLC $\gamma$ 1 signalosomes**

To further analyse CD3 $\zeta$  behaviour at the IS, we used TIRF microscopy to analyse the movement of GFP-tagged LAT-enriched vesicles in control and EB1-silenced cells. When EB1 expression is reduced, the movement of LAT-GFP vesicles at the contact area with the activating surface is impaired (Figure 5A; Supplementary Movies S7 and S8). In control T cells, LAT-GFP and CD3 $\zeta$ -Cherry-enriched vesicles co-localized upon plating on the activating surface, but this was

not seen in EB1-silenced cells (Figure 5B; Supplementary Figure S6; Supplementary Movies S9 and S10). The analysis of the movement of vesicles that appear and disappear from the TIRF plane showed that not only vesicle encounter is reduced, but that their movement is less organized, as observed in the 3D reconstruction of XY planes and time frames (Figure 5B). Analysis of LAT in EB1-silenced T lymphoblasts revealed that LAT did not accumulate at the uropod as in control cells, which relates to the increase in the LAT accumulation at the cell-cell contact in non-stimulated conjugates (Supplementary Figure S7). Upon stimulation with SEE-pulsed APCs, LAT accumulation at the IS area was decreased in EB1-silenced cells, but not abrogated. Indeed, the relative fluorescence intensity of LAT in EB1-silenced cells was also reduced with respect to control cells, suggesting that the redistribution of LAT from intracellular compartments is poorly achieved in EB1-silenced cells (Supplementary Figure S7A and B). The relationship between CD3 and LAT was further explored through specific immunoprecipitation of CD3 $\zeta$  in control T cells or EB1-silenced T cells (Figure 5C). Using specific conditions to preserve the microtubular cytoskeleton upon cell lysis, we have observed a decrease in the LAT recovery with CD3 $\zeta$  upon EB1 silencing. These results point to a role of EB1 in the organization of the IS. To analyse the activation state of T cells upon EB1 silencing, we analysed the phosphorylation of the scaffold molecule LAT. Phosphorylation of LAT on residues Y132 and Y191 was impaired in EB1-silenced T cells upon activation with HA and SEE, compared with the level in control cells (Figure 6A). In contrast, the phosphorylation level of CD3 $\zeta$  (Y83) and ZAP70 (Y493) in response to Ag (HA) or SEE activation was unaffected (Figure 6B and C). Stimulation of EB1-silenced T lymphoblasts with anti-CD3+ anti-CD28 yielded similar results (Figure 6D). Signal propagation from the stimulated TCR to LAT thus seems to be prevented when EB1 is absent.

As a further test of the role of EB1 in T cell activation we examined the activation of PLC $\gamma$ 1 at the IS by confocal microscopy of T-APC conjugates. PLC $\gamma$ 1 activation was determined by monitoring phosphorylation of residue Y783 (Poulin *et al*, 2005). Activated PLC $\gamma$ 1 was clearly localized at the IS of control T lymphoblasts, but this accumulation was prevented by EB1 depletion (Figure 7A and B). This finding was corroborated by analysis of the timing of PLC $\gamma$ 1 phosphorylation upon TCR activation, which showed that the activation of PLC $\gamma$ 1 is defective in these cells (Figure 7C). This result correlates with the lack of phosphorylation of LAT at Y132 (Figure 6A and D), where PLC $\gamma$ 1 docks upon stimulation (Paz *et al*, 2001). These results support a role for EB1 in connecting the TCR and LAT signalosomes to allow signal propagation during T cell activation.

## **Discussion**

In this study, we report the role of the +TIP MT-associated protein EB1 in IS formation and T cell activation in cells of human and mouse origin. We identify a new function for EB1 in connecting the trajectories of signalling vesicles at the IS, allowing coordinated transfer of the activation signal from the TCR to the LAT signalosomes.

The MT network organized around the MTOC has historically been viewed as a static scaffold for vesicle movement in polarized secretion (Stinchcombe and Griffiths, 2007) or for

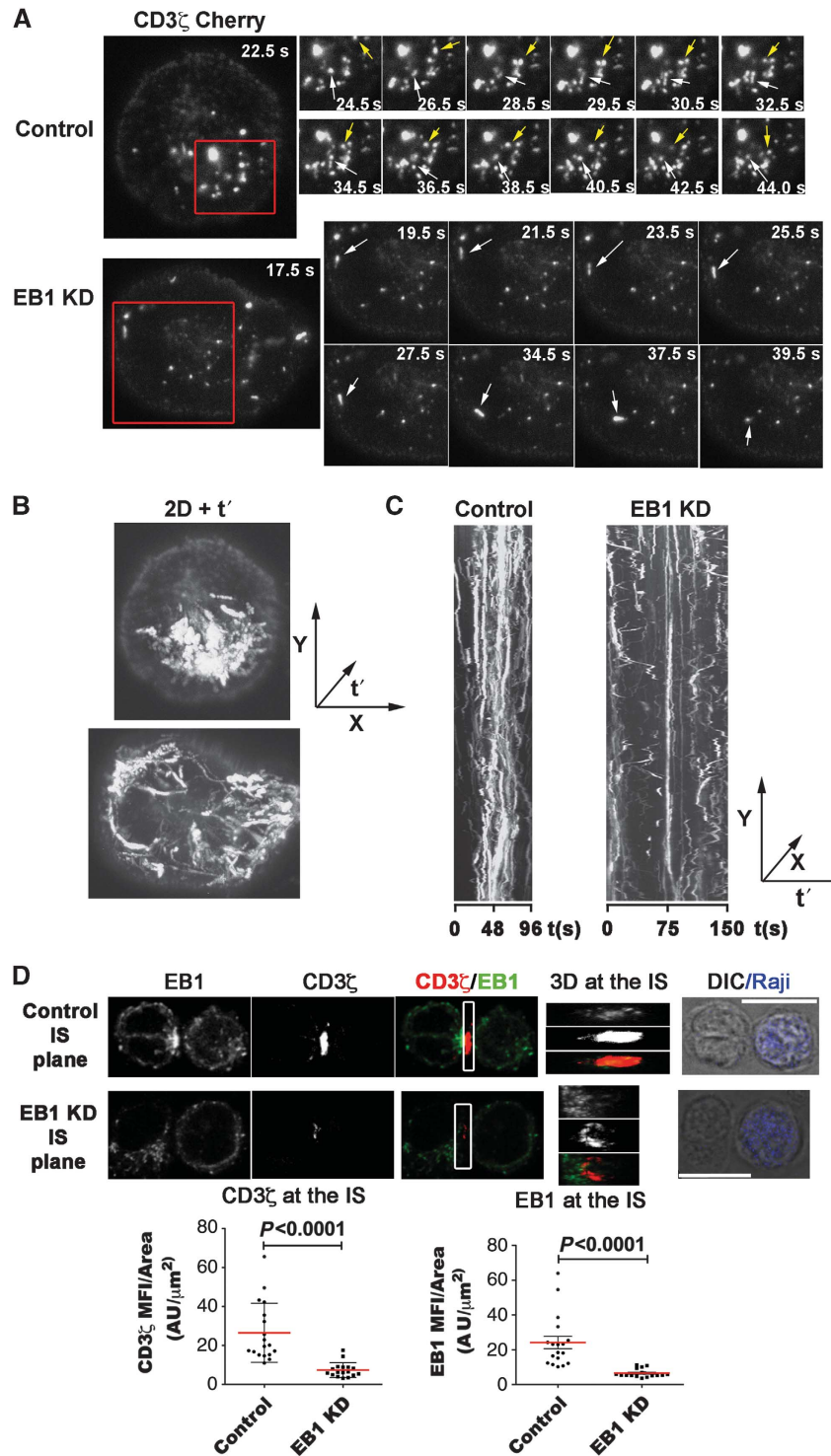


**Figure 4** EB1 regulates the trafficking of CD3 $\zeta$ -bearing vesicles at the IS. (A) shRNA-transfected (control or EB1) Jurkat T cells expressing CD3 $\zeta$ -Cherry were plated on anti-CD3 plus anti-CD28 coated glass-bottomed chambers and analysed by TIRFM. Images were taken every 500 ms at a penetrance of 110 nm. A representative cell out of at least four independent experiments is shown. (B) Maximal Z projections of the time-lapse sequences, summarizing vesicle movement in the XY plane (2D + t'). (C) Trajectory characteristics are revealed by the maximal projection of the X plane on tY plane. (D) Images showing a single confocal plane (IS plane) corresponding to control (upper panel) or EB1-silenced (EB1 KD, lower panel) T lymphoblasts conjugated with SEE-pulsed Raji cells. Cells were mixed and cultured for 30 min, fixed and stained with the indicated antibodies. Graph plots depict the distribution of mean fluorescence intensity per area of CD3 $\zeta$  and EB1 at the IS. Data are means  $\pm$  s.d. from three independent experiments (P, Mann-Whitney test).

specific signalling microclusters at the IS (Lasserre *et al*, 2010; Hashimoto-Tane *et al*, 2011). The MT network was also found to be important for maintaining the contact area of T cells with a stimulating surface (Bunnell *et al*, 2001). The

dynamics of the tubulin cytoskeleton has been analysed in T cells in terms of post-translational modifications, particularly acetylation of lysine 40 in the  $\alpha$ -tubulin subunit, which marks a population of more stable MTs

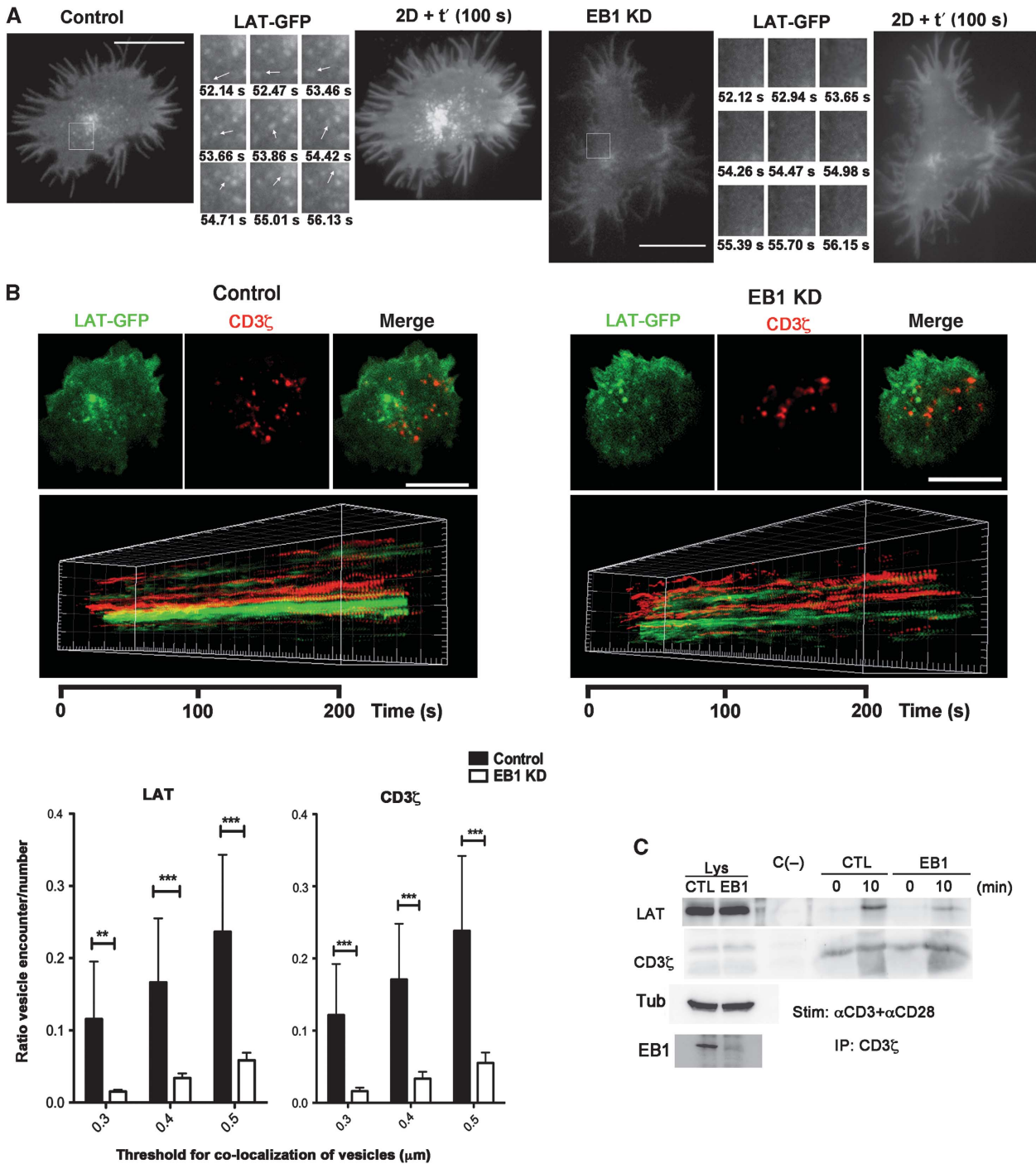


**Figure 5** Signal propagation at the IS is regulated by EB1. (A) LAT-GFP dynamics in control and EB1-silenced cells analysed by TIRFM as in Figure 4A. Images were taken every 33 (control) or 51 ms (EB1 KD) at a penetrance of 150 nm. A representative cell from out of four independent experiments is shown. (B) Analysis of LAT-GFP and CD3 $\zeta$ -Cherry dynamics in control and EB1-silenced cells by TIRFM as in Figure 3D. Images were taken every 2 s at a penetrance of 250 nm. A single time frame is shown, as well as a 3D reconstruction of time versus XY planes. Graph, vesicle encounter at the TIRFM plane. Vesicles from 100 time frames were analysed from out of 11 cells for trajectories from 5 different experiments. Images were processed for dynamics and co-localization with Imaris software (\*\*,  $P < 0.05$ ; \*\*\*,  $P < 0.001$ ; two-tailed ANOVA followed by Bonferroni posttest). (C) Co-immunoprecipitation of CD3 $\zeta$  and LAT in control and EB1-silenced cells. Cells were stimulated or not with anti-CD3 $\epsilon$  + anti-CD28 antibodies. Figure source data can be found with the Supplementary data.

(Serrador *et al*, 2004). Overexpression of histone-deacetylase 6 (HDAC6), which deacetylates acetylated  $\alpha$ -tubulin, prevents localization of the TCR at the centre of the IS and the translocation of the MTOC. CD3 $\zeta$  (Serrador *et al*, 2004) and ZAP70 (Huby *et al*, 1995) signalling components of the TCR complex have been shown to associate with  $\alpha$ -tubulin upon

TCR stimulation, and this is prevented by chemical inhibition of HDAC6 (Serrador *et al*, 2004). A specific relationship is thus established between tubulin and the TCR complex during T cell activation. However, the specific growth of MTs at the IS and the role of this process has not been addressed previously. We detected active and specific



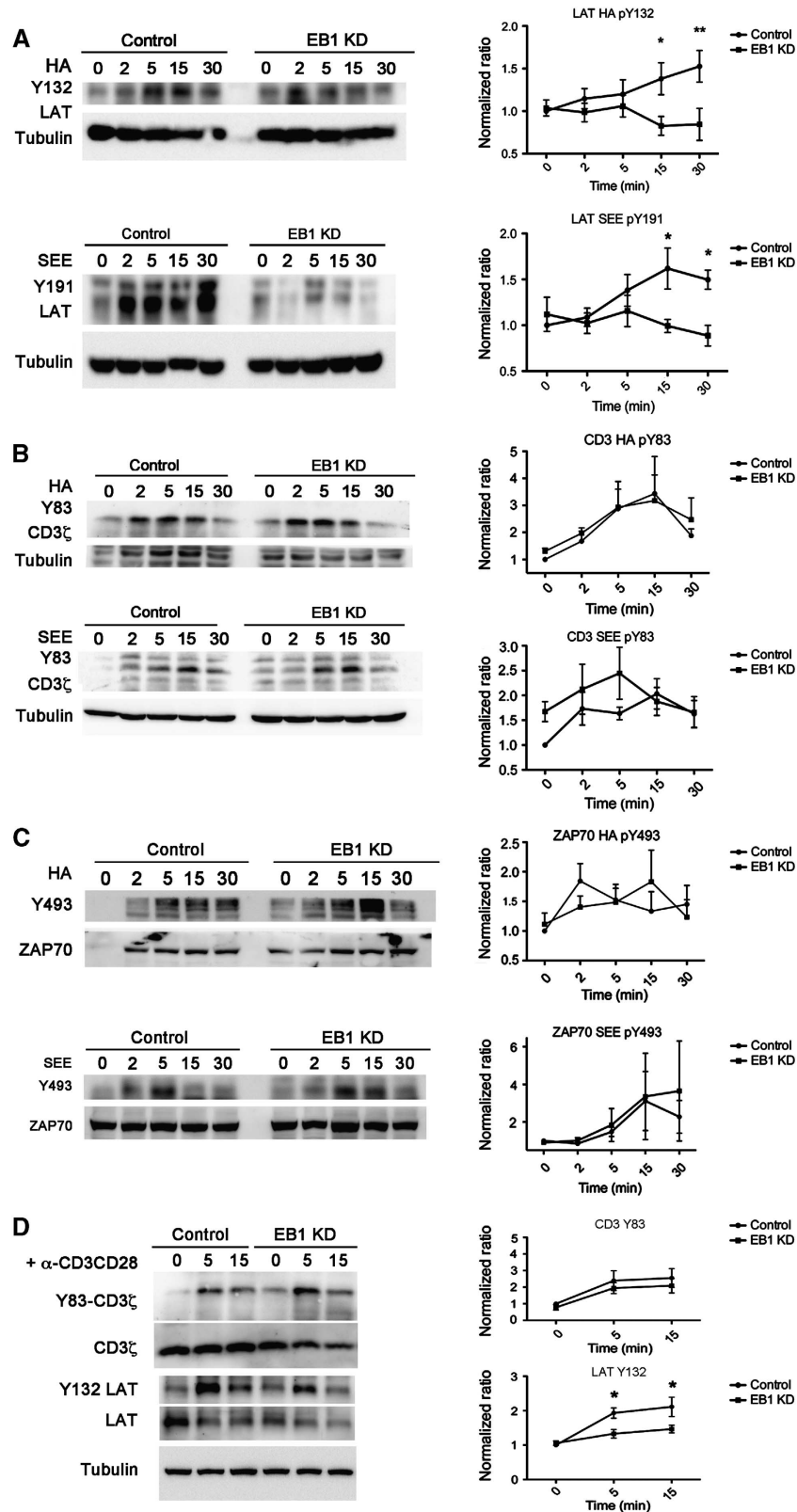


**Figure 6** Signal activation at the IS is regulated by EB1. (A) Western blot showing defective LAT activation in EB1-silenced cells CH7C17 or J77 Jurkat T cells stimulated with HA-specific peptide or SEE for the indicated times. Graphs, mean  $\pm$  s.e.m. from five and six different experiments, respectively (\*,  $P < 0.05$ ; \*\*,  $P < 0.01$ . Two-tailed ANOVA followed by Bonferroni posttests). (B, C) Western blots showing phosphorylation of CD3 $\zeta$  (B) and ZAP70 (C) in control and EB1-silenced CH7C17 or J77 Jurkat T cells stimulated with HA- or SEE-specific peptide for the indicated times. Graphs, mean  $\pm$  s.e.m. (differences were considered not significant after a two-tailed ANOVA analysis followed by Bonferroni posttests; Y83:  $N = 9$  (HA),  $N = 5$  (SEE); Y493:  $N = 4$  (HA);  $N = 3$  (SEE)). (D) Phosphorylation of CD3 $\zeta$  and LAT in control and EB1-silenced T lymphoblasts plated on anti-CD3 + anti-CD28 antibodies. A representative experiment out of at least three independent experiments is shown. Graphs, mean  $\pm$  s.e.m. from three different experiments (\*,  $P < 0.05$ ; two-tailed ANOVA followed by Bonferroni posttests). Figure source data can be found with the Supplementary data.

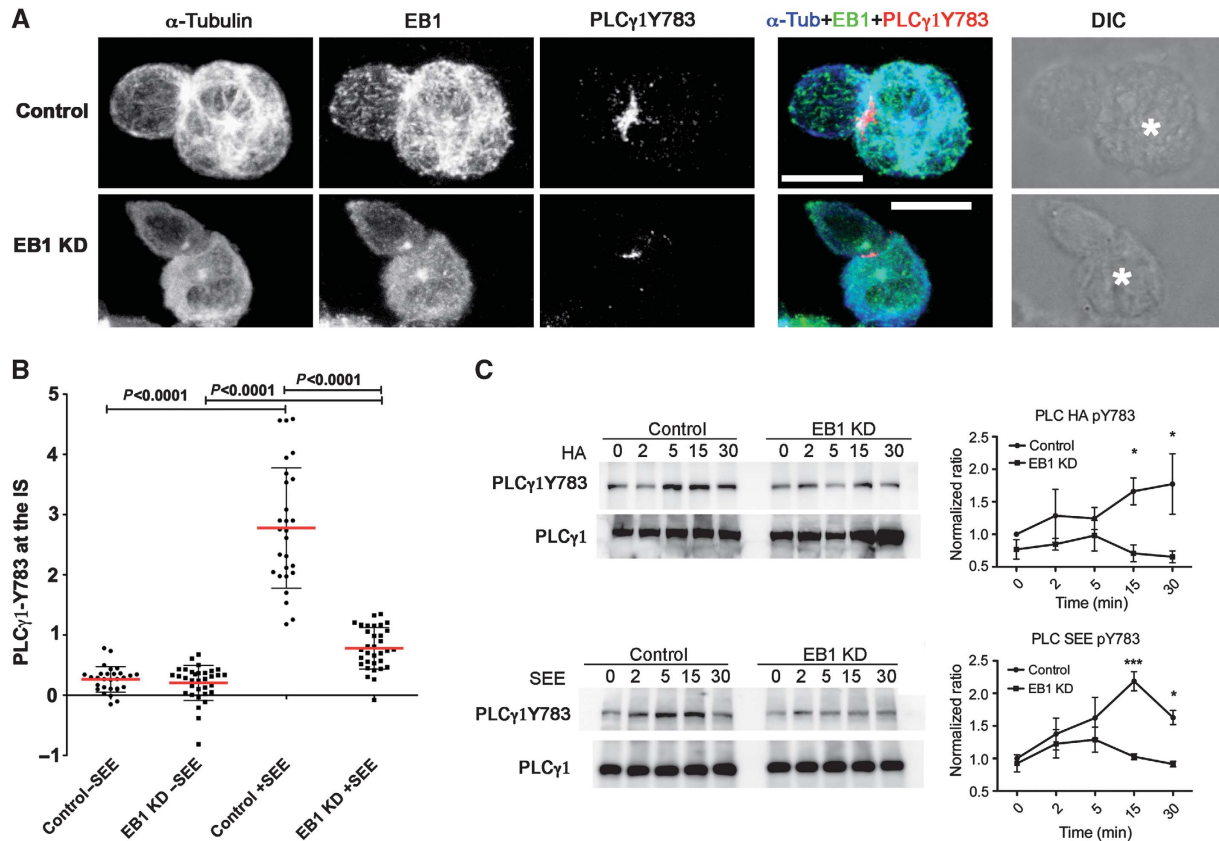


**Figure 7** PLC $\gamma$ 1 activation and clustering at the IS depends on EB1. (A) Control and EB1-silenced human T lymphoblasts were conjugated with SEE-pulsed Raji APCs, fixed and processed for immunofluorescence with the indicated antibodies. PLC $\gamma$ 1 activation was detected with the phosphospecific antibody PLC $\gamma$ 1Y783. Bar, 10  $\mu$ m. Asterisks mark SEE-pulsed Raji B cells. A representative cell conjugate out of at least three independent experiments is shown. (B) Scatter plot of the signal ratio for PLC $\gamma$ 1Y783 at the IS compared with the rest of the cell. Means  $\pm$  s.d. from three independent experiments are depicted. Data were analysed with Mann-Whitney test. (C) Western blot showing the effect of EB1 knockdown on the timing of PLC $\gamma$ 1 Y783 phosphorylation in CH7C17 Jurkat T cells stimulated with HA-specific peptide and in T lymphoblasts stimulated with SEE (\*,  $P < 0.05$ , \*\*\*,  $P < 0.001$ ). Two-tailed ANOVA followed by Bonferroni posttests.  $N = 4$  (HA) and  $N = 3$  (SEE). Figure source data can be found with the Supplementary data.

tubulin polymerization at the IS, paralleling the localized polymerization of actin (Gomez and Billadeau, 2008). Our data show that the centrosome of the activated T lymphocyte is very active as a centre of tubulin polymerization (MTOC) upon TCR engagement, and its translocation to the IS facilitates the localization of newly polymerized MTs to this active cellular location. These MTs may serve to guide the trafficking of specific vesicles at the IS to the plasma membrane and from the plasma membrane to intracellular compartments since inhibition of MT growth through specific knock-down of EB1 (Komarova *et al*, 2009), prevents the correct movement of vesicles. Other foci of MT growth, unrelated to the centrosome and the Golgi Apparatus (Vinogradova *et al*, 2009), may contribute to intracellular traffic at the IS and further studies should elucidate their role.

EB1 is composed of two well-differentiated domains: a globular CH domain that encompasses the N-terminal half of the protein and binds to MTs, and a C-terminal homodimerization domain. In the EB1 homodimer, the C-terminal domain adopts a novel coiled-coil, four-helix bundle conformation. Our results show that EB1 interacts through this four-helix bundle domain with the ITAM of CD3 $\epsilon$  and the ITAMs of CD3 $\zeta$ . This interaction may underlie the ability of EB1-decorated MT plus-ends to bind TCR-bearing vesicles, promoting their movement in and out of the IS plane.

Interestingly, the movement of the vesicles is erratic when EB1 expression is reduced, and corresponds to the localization of accumulated, peripheral clusters of TCR in fixed cell conjugates.

Our results reveal that signals from the TCR signalosome (Guy and Vignali, 2009) cannot propagate to the LAT/PLC $\gamma$ 1 cassette when EB1-dependent tracking of MTs is disrupted, supporting the notion that a continuously remodelled microtubular network is essential for the trafficking of vesicles at the IS. Moreover, TCR and LAT vesicles appear to be different and must encounter each other to allow the specific propagation of activation signals. These effects are very rapid and can be observed readily after T cell activation, correlating with the described effect of HDAC6 on tubulin dynamics upon TCR engagement (Serrador *et al*, 2004). The backward trafficking to intracellular compartments of vesicles docked at MT plus-tips is in accord with a recently proposed model (Akhmanova and Hammer, 2010), in which dynein/dynactin molecular motors would drive movement toward the minus end of the MTs (the centrosome). In this regard, EB1 C terminus ends with an acidic stretch that has been described as the binding site for p150<sup>Glued</sup>, a dynactin subunit (Manna *et al*, 2008). Therefore, EB1 localized at MT plus-ends may help the interaction of TCR and thus CD3 $\zeta$ -enriched vesicles with dynein/dynactin motors.

A dynein/dynactin-driven movement would promote the movement of vesicles along MTs towards their minus-end, the centrosome, where the Golgi is organized. The multi-vesicular bodies found at the IS (Calabia-Linares *et al*, 2011; Mittelbrunn *et al*, 2011) might also be the fate of the TCR-containing vesicles, on their way to recycling or degradation pathways. Early endosomal compartments may also be attained through MT-driven trafficking (Nielsen *et al*, 1999).

The failure of MTOC translocation in dynein/dynactin-disrupted T cells of human origin (Martin-Cofreces *et al*, 2008) would prevent the tubulin polymerization at the IS observed here, preventing correct movement of vesicles towards intracellular compartments. The predicted outcome would be accumulation of TCR at the periphery of the IS instead of forming a central cluster, as observed (Martin-Cofreces *et al*, 2008). The tubulin cytoskeleton and related proteins therefore appear to be of critical importance for the formation of the IS and sustained T cell activation. In this regard, a recent report has identified casein kinase I  $\delta$  (CKI $\delta$ ) as an important molecule controlling MTOC translocation to the IS and MT growing. CKI $\delta$  can bind to EB1 and the region of CKI $\delta$  implicated in this interaction is required for MTOC translocation (Zyss *et al*, 2011). Therefore, EB1 localization at the MTOC may be determined by CKI $\delta$ , and its plus-end tracking activity regulated by the kinase through phosphorylation to promote the MT growing observed herein. However, the absence of CKI $\delta$  does neither affect IS architecture nor signalling (Zyss *et al*, 2011), which points to other complementary mechanisms to regulate EB1 function.

We found that vesicle movement is important for correct activation of signalling via LAT and PLC $\gamma$ 1. Phosphorylation of these proteins on key residues was decreased in EB1-silenced cells, even though the rate of phosphorylation of CD3 $\zeta$  and ZAP70 was similar to control cells. LAT phosphorylation during T cell spreading and its correspondence with microclusters has been shown to be relevant during T cell activation (Campi *et al*, 2005). Indeed, the relative movement of LAT microclusters with respect to LAT vesicles has also been shown to be important for correct T cell activation (Purbhoo *et al*, 2010). Our results show that the coordinated movement and correct encounter between CD3 $\zeta$ - and LAT-enriched vesicles is necessary for signal propagation from the TCR. This movement may help the relationship between the described protein islands for TCR and LAT (Lillemeier *et al*, 2010). The specific contribution of MTOC translocation to the localization of vesicles at the IS and subsequent MT polymerization warrants further research.

## Materials and methods

### Cells, plasmids and cell transfection

All primary healthy donor samples were obtained after written consent, in accordance with the Declaration of Helsinki, and approved by the Hospital La Princesa Research Ethics Committee. Human T lymphoblasts were obtained from peripheral blood lymphocytes (PBLs) isolated from freshly prepared buffy coats. Buffy coats were subjected to gradient centrifugation on Histopaque-1077 from Sigma-Aldrich (St Louis, MO, USA), followed by two rounds of plastic adherence. SEE-specific human T lymphoblasts were obtained as described (Ibiza *et al*, 2006). V $\beta$ 8 + Jurkat T cell clones (J77) and the lymphoblastoid Raji and Hom2 B cell lines were cultured in complete medium. HA-specific, V $\beta$ 3 + Jurkat T cells (CH7C17) were supplemented with 400  $\mu$ g/ml hygromycin B and

4  $\mu$ g/ml puromycin (Martin-Cofreces *et al*, 2008). T lymphoblasts were isolated by negative selection using the AutoMACS cell separation system (Miltenyi Biotec GmbH, Bergisch Gladbach, Germany). The cDNA encoding N-terminal GFP-linked EB1 was a kind gift from Anna Akhmanova (Utrecht University, The Netherlands). LAT-GFP was as described (Bonello *et al*, 2004). The indicated cDNAs were transiently transfected into T cells ( $2 \times 10^7$ ) with the Bio-Rad Gene Pulser II electroporation system. At 16 h post transfection, viable T lymphoblasts, J77 or CH7C17 cells were isolated by centrifugation on a Ficoll-Hypaque gradient and conjugated with Raji (T lymphoblasts and J77 cells) or Hom2 cells (CH7C17 cells) for functional studies. EB1-silencing assays were performed as follows: J77 or CH7C17 T cells were electroporated with a shRNA plasmid encoding a specific 21 bp sequence against EB1 (GACATGACATGCTGGCCTGCG) or with the corresponding control plasmid encoding a negative sequence (TGGCATTGTCTTACCGCCTAT) (Genscript, Piscataway, NJ, USA), or instead with a double-stranded control siRNA or a specific sequence against EB1 (CAGACAAGGUCAAGAAACU and CGUACGCGGAAUACUUCGA, respectively; Eurogentec, San Diego, CA, USA) at a final concentration of 2  $\mu$ M per sample. Cells were then collected and the efficiency of gene silencing assessed by western blot. Cells were used for experiments on day three post electroporation with shRNA or the day after electroporation with siRNA. For TIRFM analyses, cells were re-electroporated with shRNA and plasmids for LAT-GFP and/or CD3 $\zeta$ -Cherry after 3 days of cell culture with 0.75 mg/ml G418 as selection antibiotic and used the following day.

### Yeast two-hybrid assay

To characterize new CD3 $\epsilon$ -interacting partners, we used the yeast two-hybrid SOS-recruitment system (Gil *et al*, 2002). The sequence encoding the human CD3 $\epsilon$  cytoplasmic tail was amplified by PCR with end primers that add *Nco*I and *Sac*I flanking restriction sites, and was cloned into the plasmid pSOS (Stratagene) to yield pSOS-CD3 $\epsilon$ . As a bait we used the construct pSOS-CD3 $\epsilon$  Tandem containing two copies in tandem, head to tail, of the cytoplasmic tail of CD3 $\epsilon$ . The control constructs pSOS-MafB, pMyr-MafB and pMyr-LamC were provided by Stratagene. The bait construct was transfected in the *cdc25* yeast mutant together with a human spleen cDNA library made in the pMyr vector (Stratagene) and the transfectants ( $3 \times 10^6$ ) were selected at the restrictive temperature (37°C) in a manner dependent of galactose, and not glucose, as a carbon source. Of the 319 resulting colonies, 304 were discarded as revertants of the *cdc25* mutation since they grew in the presence of glucose. The pMyr plasmid was isolated of the remaining 15 clones and assayed in regard to their ability to promote the growth in galactose at 37°C in the presence of the empty pSOS vector. Only two clones did not grow in these conditions, one contained a cDNA encoding for Nck- $\beta$  (Gil *et al*, 2002); the other for the last 82 amino acids of EB1.

### Antibodies and reagents

T3b (anti-human-CD3) was produced in the laboratory. Rabbit polyclonal Ab 448 (anti-human-CD3 $\zeta$ ) has been described previously (San Jose *et al*, 1998). Anti-human V $\beta$ 8 was from BD Biosciences/Clontech (San Jose, CA, USA). Unconjugated and FITC-conjugated anti- $\alpha$ -tubulin, phalloidin and GCP3 rabbit polyclonal were from Sigma-Aldrich. Anti-LAT was from Santa Cruz Biotechnology, Inc. (Santa Cruz, CA, USA). Anti-phospho-LAT (Y191) was from Millipore (Billerica, MA, USA), and anti-phospho-LAT (Y132) was from Abcam (Cambridge, MA, USA). Anti-phospho-PLC $\gamma$ -1 (Y783), anti-PLC $\gamma$ -1 and anti-phospho-PKC $\theta$  (T538) were from Cell Signaling Technology (Danvers, MA, USA). Anti-phospho-CD3z (Y83) was from Epitomics (Burlingame, CA, USA).

Human fibronectin and poly-L-lysine (PLL) were from Sigma-Aldrich, SEE from Toxin Technology (Sarasota, FL, USA), puromycin from InvivoGen (San Diego, CA, USA), and hygromycin B from Roche Diagnostics GmbH (Penzberg, Germany). Anti-Erk 1/2 and the fluorescent secondary antibodies (Alexa 568 and 647, and rhodamine red X) and cell trackers (7-amino-4-chloromethylcoumarin (CMAC), 5-(and-6)-(((4-chloromethyl) benzoyl) amino) tetramethylrhodamine (CMTMR)) were obtained from Invitrogen (Carlsbad, CA, USA). Propidium iodide was from Sigma-Aldrich. All other reagents were of the purest grade available.

**Cell conjugate formation and immunofluorescence analysis**

Raji B cells were loaded with the blue fluorescent cell tracker CMAC. Cells were then incubated in HBSS for 30 min with or without 0.5 µg/ml SEE, centrifuged at low speed, and allowed to form conjugates with J77 Jurkat cells or SEE-CD4 human primary T cells during incubation for 20 min at 37°C. Hom2 cells were also loaded with CMAC, incubated for 2 h with 50 µg/ml HA peptide, and allowed to form conjugates with CH7C17 cells. In these assays, the T cells ( $2 \times 10^5$ ) were mixed with an equal number of APCs in a final volume of 80 µl, gently resuspended, and plated onto slides coated with PLL (Jurkat) or FN (CH7C17). Cells were fixed with a mix of paraformaldehyde and methanol for 4 min at  $-20^\circ\text{C}$  and permeabilized when needed for 5 min in 2% paraformaldehyde and 0.2% Triton X-100 in PHEM/saccharose, blocked and stained with the indicated Abs. Stained cells were mounted in a mowiol-based mounting solution (ProLong Gold antifade reagent; Invitrogen) and observed under a confocal laser scanning unit (TCS SP5; Leica) attached to an inverted epifluorescence microscope (DMI6000; Leica) fitted with an HCX PL APO 63 × /1.40-0.6 oil objective. Images were acquired and processed with accompanying confocal software (LCS; Leica) or WCIF ImageJ (<http://rsbweb.nih.gov/ij/>). 3D analysis and maximal projections of the T cell-APC contact area were generated with ImageJ to obtain a z stack projection. Figures were composed with Photoshop CS4.

**Analysis of CD3ζ, LAT and PLCγ1 accumulation at the T-APC contact area**

T-APC conjugates were formed, fixed and analysed by confocal imaging as indicated above and images were analysed with ImageJ. We assumed that protein accumulation was homogeneous in the APC when present, with no additional accumulation at the contact zone with the T cell. For quantification in individual ISs we used a home-made plugin for ImageJ (<http://rsbweb.nih.gov/ij/>) called 'Synapse Measures'. By comparing fluorescence signals from multiple regions of the T cell, APC, IS, and background fluorescence, the program yields accurate measurements of localized immunofluorescence. A detailed description of *Synapse Measures*, including the algorithms used, is described (Calabia-Linares *et al*, 2011).

**Time-lapse fluorescence confocal microscopy and TIRFM**

Raji APCs ( $5 \times 10^5$ ; SEE-pulsed or unpulsed) were allowed to adhere to FN coated coverslips in Attofluor open chambers (Invitrogen) at 37°C in a 5% CO<sub>2</sub> atmosphere. The cells were maintained in 1 ml HBSS (2% BSA). T cells were added (1:1 ratio) and a series of fluorescence and differential interference contrast frames were captured using a TCS SP5 confocal laser scanning unit attached to an inverted epifluorescence microscope (DMI6000) fitted with an HCX PL APO 63 × /1.40-0.6 oil objective. Images were acquired and processed with the accompanying confocal software (LCS; Leica). Premiere 6.0 software (Adobe) was used to generate QuickTime videos (Apple).

For TIRFM, T cells transfected with CD3ζ-Cherry, LAT-GFP, and control or shEB1 plasmid were allowed to settle onto CD3 plus CD28 coated glass bottomed microwell dishes, No 1.5 (Mattek, Ashland, MA, USA). Recording was initiated 3 min after cells were plated and cells were visualized with a Leica AM TIRF MC M mounted on a Leica DMI 6000B microscope coupled to an Andor-DU8285\_VP-4094 camera. Images were acquired with a HCX PL APO 100.0 × 1.46 OIL objective and processed with the accompanying confocal software (LCS; Leica). For vesicle tracking, penetration was 150 or 250 nm for both laser channels (488 and 561 nm) with same objective angle. Synchronization was performed through the Leica software.

**GST-pull down, immunoprecipitation, centrosomal isolation and immunoblotting**

For GST-pull down, corresponding recombinant GST protein was added to cell lysates and pull down performed as described (Urzainqui *et al*, 2002). For immunoprecipitation, T cells were

stimulated with corresponding Ag or Sag-pulsed APCs (ratio 1:5) or antibodies (anti-CD3 or anti-CD3 + anti-CD28) for the indicated times and lysed in 20 mM Tris-HCl, pH 7.5, 150 mM NaCl buffer containing 1% Brj96 and phosphatase and protease inhibitors in non-reducing conditions. Anti-HA tag antibody, anti-CD3ζ rabbit anti-serum or anti-EB1 antibody were used for immunoprecipitation. For LAT and CD3ζ co-immunoprecipitation, cells were silenced for EB1 and stimulated or not with anti-(CD3ε + CD28) antibody-coated beads. The complete procedure was performed at room temperature. Cells were lysed on PHEM buffer (60 mM PIPES, 25 mM Hepes, 5 mM EGTA, 2 mM MgCl<sub>2</sub>) with 0.33% Brij 96v supplemented with protease and phosphatase inhibitors. Preclearing and antibody recovery were performed using the Protein-G magnet beads from Millipore. Anti-CD3ζ rabbit anti-serum was used for immunoprecipitation during 2 h. Blots were revealed using True Blot reagent for detection of primary antibodies. Centrosomal isolation was performed from control or anti-CD3-stimulated CH7C17 T cells as described (Bornens and Moudjou, 1999). For analysis of protein phosphorylation during formation of the IS, Raji or Hom2 cells ( $1 \times 10^6$ ) were preloaded with 0.5 µg/ml SEE or 50 µg/ml HA peptide at 37°C for 30 min or 2 h and mixed with  $5 \times 10^6$  Jurkat or CH7C17 cells at 37°C, respectively. After incubation, cells were lysed at 4°C for 40 min in 50 mM Tris-HCl, pH 7.5, containing 1% NP-40, 0.2% Triton X-100, 150 mM NaCl, and phosphatase and protease inhibitors. Cell lysates were spun at 2500g for 10 min to remove cell debris and nuclei. GST-pull downs, immunoprecipitates, centrosomal fractions and whole lysates were analysed by SDS-PAGE, transferred onto nitrocellulose membranes, and probed with the indicated antibodies in TBS-Tween-20. Bound antibodies were reacted with HRP secondary antibodies, and membranes were developed by enhanced chemiluminescence with SuperSignal West Pico or Femto chemiluminescent substrate (Pierce). Densitometric analyses were performed with ImageGauge 3.46 software (Fujifilm).

**Statistical analysis**

Data were tested for normality using the D'Agostino-Pearson omnibus normality test, or the Kolmogorov-Smirnov test when the sample was small. Differences between means were tested by Student's *t*-test for normal data, while non-normal data were analysed by the Mann-Whitney test. Two-tailed ANOVA was used for grouped data, followed by Bonferroni post-test. GraphPad Prism software was used for statistical analyses.

**Supplementary data**

Supplementary data are available at *The EMBO Journal* Online (<http://www.embojournal.org>).

**Acknowledgements**

We thank S Bartlett for editorial support and critical reading of the manuscript. This work was supported by grants from Spanish Ministry of Science and Innovation (SAF2011-25834 to FSM, SAF2010-14912 to BA and grants to FB and NBMC), INDISNET S2011/BMD-2332 to FSM and BA from Comunidad de Madrid and ERC-2011-AdG 294340-GENTRIS. The Centro Nacional de Investigaciones Cardiovasculares (CNIC, Spain) is supported by the Spanish Ministry of Science and Innovation and the Pro-CNIC Foundation.

*Author contributions:* NBMC, FB, BA and FSM designed experimentation and analysed results; NBMC, FB, MJ, DG and AM collected and analysed the data; NBMC made the figures and wrote the manuscript with input from FB, BA and FSM.

**Conflict of interest**

The authors declare that they have no conflict of interest.

**References**

- Akhmanova A, Hammer 3rd JA (2010) Linking molecular motors to membrane cargo. *Curr Opin Cell Biol* **22**: 479–487  
 Akhmanova A, Steinmetz MO (2008) Tracking the ends: a dynamic protein network controls the fate of microtubule tips. *Nat Rev Mol Cell Biol* **9**: 309–322

- Askham JM, Vaughan KT, Goodson HV, Morrison EE (2002) Evidence that an interaction between EB1 and p150(Glued) is required for the formation and maintenance of a radial microtubule array anchored at the centrosome. *Mol Biol Cell* **13**: 3627–3645

- Baixauli F, Martín-Cofreces NB, Morlino G, Carrasco YR, Calabia-Linares C, Veiga E, Serrador JM, Sánchez-Madrid F (2011) The mitochondrial fission factor dynamin-related protein 1 modulates T-cell receptor signalling at the immune synapse. *EMBO J* **30**: 1238–1250
- Bettencourt-Dias M, Glover DM (2007) Centrosome biogenesis and function: centrosomes brings new understanding. *Nat Rev Mol Cell Biol* **8**: 451–463
- Bonello G, Blanchard N, Montoya MC, Aguado E, Langlet C, He HT, Nunez-Cruz S, Malissen M, Sanchez-Madrid F, Olive D, Hivroz C, Collette Y (2004) Dynamic recruitment of the adaptor protein LAT: LAT exists in two distinct intracellular pools and controls its own recruitment. *J Cell Sci* **117**: 1009–1016
- Bornens M, Moudjou M (1999) Studying the composition and function of centrosomes in vertebrates. *Methods Cell Biol* **61**: 13–34
- Bunnell SC, Kapoor V, Triple RP, Zhang W, Samelson LE (2001) Dynamic actin polymerization drives T cell receptor-induced spreading: a role for the signal transduction adaptor LAT. *Immunity* **14**: 315–329
- Calabia-Linares C, Robles-Valero J, De La Fuente H, Perez-Martínez M, Martín-Cofreces NB, Alfonso-Pérez M, Gutiérrez-Vázquez C, Mittelbrunn M, Ibiza S, Urbano-Olmos FR, Aguado-Ballano C, Sánchez-Sorzano CO, Sánchez-Madrid F, Veiga E (2011) Endosomal clathrin drives actin accumulation at the immunological synapse. *J Cell Sci* **124**: 820–830
- Campi G, Varma R, Dustin ML (2005) Actin and agonist MHC-peptide complex-dependent T cell receptor microclusters as scaffolds for signaling. *J Exp Med* **202**: 1031–1036
- Etienne-Manneville S (2010) From signaling pathways to microtubule dynamics: the key players. *Curr Opin Cell Biol* **22**: 104–111
- Gil D, Schamel WW, Montoya M, Sanchez-Madrid F, Alarcon B (2002) Recruitment of Nck by CD3 epsilon reveals a ligand-induced conformational change essential for T cell receptor signaling and synapse formation. *Cell* **109**: 901–912
- Gomez TS, Billadeau DD (2008) T cell activation and the cytoskeleton: you can't have one without the other. *Adv Immunol* **97**: 1–64
- Grigoriev I, Akhmanova A (2010) Microtubule dynamics at the cell cortex probed by TIRF microscopy. *Methods Cell Biol* **97**: 91–109
- Guy CS, Vignali DA (2009) Organization of proximal signal initiation at the TCR:CD3 complex. *Immunol Rev* **232**: 7–21
- Hashimoto-Tane A, Yokosuka T, Sakata-Sogawa K, Sakuma M, Ishihara C, Tokunaga M, Saito T (2011) Dynein-driven transport of T cell receptor microclusters regulates immune synapse formation and T cell activation. *Immunity* **34**: 919–931
- Huby RD, Carlisle GW, Ley SC (1995) Interactions between the protein-tyrosine kinase ZAP-70, the proto-oncoprotein Vav, and tubulin in Jurkat T cells. *J Biol Chem* **270**: 30241–30244
- Huse M, Quann EJ, Davis MM (2008) Shouts, whispers and the kiss of death: directional secretion in T cells. *Nat Immunol* **9**: 1105–1111
- Ibiza S, Victor VM, Bosca I, Ortega A, Urzainqui A, O'Connor JE, Sanchez-Madrid F, Esplugues JV, Serrador JM (2006) Endothelial nitric oxide synthase regulates T cell receptor signaling at the immunological synapse. *Immunity* **24**: 753–765
- Komarova Y, De Groot CO, Grigoriev I, Gouveia SM, Munteanu EL, Schober JM, Honnappa S, Buey RM, Hoogenraad CC, Dogterom M, Borisy GG, Steinmetz MO, Akhmanova A (2009) Mammalian end binding proteins control persistent microtubule growth. *J Cell Biol* **184**: 691–706
- Lasserre R, Charrin S, Cuhe C, Danckaert A, Thoulouze MI, de Chaumont F, Duong T, Perrault N, Varin-Blank N, Olivo-Marin JC, Etienne-Manneville S, Arpin M, Di Bartolo V, Alcover A (2010) Ezrin tunes T-cell activation by controlling Dlg1 and microtubule positioning at the immunological synapse. *EMBO J* **29**: 2301–2314
- Li R, Gundersen GG (2008) Beyond polymer polarity: how the cytoskeleton builds a polarized cell. *Nat Rev Mol Cell Biol* **9**: 860–873
- Lillemeier BF, Mortelmaier MA, Forstner MB, Huppa JB, Groves JT, Davis MM (2010) TCR and Lat are expressed on separate protein islands on T cell membranes and concatenate during activation. *Nat Immunol* **11**: 90–96
- Lowin-Kropf B, Shapiro VS, Weiss A (1998) Cytoskeletal polarization of T cells is regulated by an immunoreceptor tyrosine-based activation motif-dependent mechanism. *J Cell Biol* **140**: 861–871
- Manna T, Honnappa S, Steinmetz MO, Wilson L (2008) Suppression of microtubule dynamic instability by the + TIP protein EB1 and its modulation by the CAP-Gly domain of p150glued. *Biochemistry* **47**: 779–786
- Martin-Cofreces NB, Robles-Valero J, Cabrero JR, Mittelbrunn M, Gordon-Alonso M, Sung CH, Alarcon B, Vazquez J, Sanchez-Madrid F (2008) MTOC translocation modulates IS formation and controls sustained T cell signaling. *J Cell Biol* **182**: 951–962
- Martin-Cofreces NB, Sancho D, Fernandez E, Vicente-Manzanares M, Gordon-Alonso M, Montoya MC, Michel F, Acuto O, Alarcon B, Sanchez-Madrid F (2006) Role of Fyn in the rearrangement of tubulin cytoskeleton induced through TCR. *J Immunol* **176**: 4201–4207
- Mittelbrunn M, Gutierrez-Vazquez C, Villarroya-Beltri C, Gonzalez S, Sanchez-Cabo F, Gonzalez MA, Bernad A, Sanchez-Madrid F (2011) Unidirectional transfer of microRNA-loaded exosomes from T cells to antigen-presenting cells. *Nat Commun* **2**: 282
- Nielsen E, Severin F, Backer JM, Hyman AA, Zerial M (1999) Rab5 regulates motility of early endosomes on microtubules. *Nat Cell Biol* **1**: 376–382
- Paz PE, Wang S, Clarke H, Lu X, Stokoe D, Abo A (2001) Mapping the Zap-70 phosphorylation sites on LAT (linker for activation of T cells) required for recruitment and activation of signalling proteins in T cells. *Biochem J* **356**: 461–471
- Poulin B, Sekiya F, Rhee SG (2005) Intramolecular interaction between phosphorylated tyrosine-783 and the C-terminal Src homology 2 domain activates phospholipase C-gamma1. *Proc Natl Acad Sci USA* **102**: 4276–4281
- Purbhoo MA, Liu H, Oddos S, Owen DM, Neil MA, Pigeon SV, French PM, Rudd CE, Davis DM (2010) Dynamics of subsynaptic vesicles and surface microclusters at the immunological synapse. *Sci Signal* **3**: ra36
- San Jose E, Sahuquillo AG, Bragado R, Alarcon B (1998) Assembly of the TCR/CD3 complex: CD3 epsilon/delta and CD3 epsilon/gamma dimers associate indistinctly with both TCR alpha and TCR beta chains. Evidence for a double TCR heterodimer model. *Eur J Immunol* **28**: 12–21
- San Jose E, Alarcon B (1999) Receptor engagement transiently diverts the T cell receptor heterodimer from a constitutive degradation pathway. *J Biol Chem* **274**: 33740–33746
- Schamel WW, Risueno RM, Minguet S, Ortiz AR, Alarcon B (2006) A conformation- and avidity-based proofreading mechanism for the TCR-CD3 complex. *Trends Immunol* **27**: 176–182
- Serrador JM, Cabrero JR, Sancho D, Mittelbrunn M, Urzainqui A, Sanchez-Madrid F (2004) HDAC6 deacetylase activity links the tubulin cytoskeleton with immune synapse organization. *Immunity* **20**: 417–428
- Sigalov AB (2006) Immune cell signaling: a novel mechanistic model reveals new therapeutic targets. *Trends Pharmacol Sci* **27**: 518–524
- Stinchcombe JC, Griffiths GM (2007) Secretory mechanisms in cell-mediated cytotoxicity. *Annu Rev Cell Dev Biol* **23**: 495–517
- Tirnauer JS, Bierer BE (2000) EB1 proteins regulate microtubule dynamics, cell polarity, and chromosome stability. *J Cell Biol* **149**: 761–766
- Urzainqui A, Serrador JM, Viedma F, Yanez-Mo M, Rodriguez A, Corbi AL, Alonso-Lebrero JL, Luque A, Deckert M, Vazquez J, Sanchez-Madrid F (2002) ITAM-based interaction of ERM proteins with Syk mediates signaling by the leukocyte adhesion receptor PSGL-1. *Immunity* **17**: 401–412
- van der Merwe PA, Dushek O (2011) Mechanisms for T cell receptor triggering. *Nat Rev Immunol* **11**: 47–55
- Vinogradova T, Miller PM, Kaverina I (2009) Microtubule network asymmetry in motile cells: role of Golgi-derived array. *Cell Cycle* **8**: 2168–2174
- Zyss D, Ebrahimi H, Gergely F (2011) Casein kinase I delta controls centrosome positioning during T cell activation. *J Cell Biol* **195**: 781–797